33rd Annual International Conference of the IEEE EMBS
Boston, Massachusetts USA, August 30 - September 3, 2011

# Boundary Delineation for Hepatic Hemangioma In ultrasound images

Naeim Bahrami, Seyed Hamid Rezatofighi, Aliyeh Mahdavi Adeli, and S. Kamaledin Setarehdan
Control and Intelligent Processing Center of Excellence, School of
Electrical and Computer Engineering, Faculty of Engineering, University of
Tehran, Tehran, Iran

***Abstract - Hemangioma is one of the most common benign congenital complications of the human body which can arise in interior organs and external limbs. The main aim of this work is to present a new method for automatic detection of liver hemangioma and its boundaries in ultrasound images, using image processing techniques. Overall there are two phases, the preprocessing procedure and the boundary delineation phase. The preprocessing phase includes three main stages: 1. Image contrast enhancement using Difference of Offset Gaussian (DoOG) method, 2. Applying Canny edge filtering , 3. Applying an adaptive threshold in order to detect the ROI (hemangioma).Following, the snake algorithm is used to segment the hemangioma region in the second phase. For the quantitative assessment of the proposed method for the segmentation stage, the results derived via the proposed algorithms have been compared with the corresponding segmented regions determined by an expert using three similarity criteria. The results showed 73 percent similarity without pre-processing and 90 percent similarity with pre-processing.***

***Keywords: Active contour model, Difference of offset Gaussian, Hemangioma, Image processing, Liver, Ultrasound.***

## I. INTRODUCTION

Hemangioma is an unusual formation of blood vessels in the skin or internal organs which is considered a benign (non-malignant) congenital complication. Approximately 20% of hemangioma lumps appear and form in the liver causing problems for the affected individual. According to the literature [1], this lesion is the most common type of hepatic tumors. Effects of hemangioma can be wounds, bleedings and pain in the specific area. Wrong detection of such a lesion can cause an unnecessary surgery for the patient whereas an on time and exact detection of this disease can enable the treatment of it with low risk and less cost. The chances for early clinical assessment of hepatic Hemangioma by employing biopsy is often small and almost impossible because of its hyper vascular structure. Ultrasound imaging and scanning of the liver are, therefore, commonly utilized as the routine methods of liver tumor detection and diagnosis [1].

Engineering enhancements over the years have resulted in improved qualitative visual inspection of ultrasound images in real-time by a trained physician [2]. In spite of recent advances in ultrasonic imaging, manual boundary delineation of tumors in hepatic images by physicians is still a challenging task due to poor contrast, missing boundary, low SNR, speckle noise and refraction of the images [3]. Previous studies on liver images have demonstrated that visual interpretation of gray scale images is not highly accurate in identifying these lesions and is not suitably discriminating between hemangiomas and other hepatic tumors. This limitation is partially due to the fact that the human eye is capable of distinguishing only about 30 gray tones between black and white [2]. Thus, automated boundary delineation that can overcome such weaknesses and subjectivity of the observer's interpretation of ultrasound images, is essential for the early detection and treatment of hepatic hemangioma.

Ultrasound image segmentation is one of the most challenging tasks in ultrasound image analysis methods. One of the reasons for such problems is speckle noise existence which makes it unreliable to classify image pixels [3], because it makes clear edges hard to detect. Most image segmentation methods focus on region growing or active contours. The active contour methods are designed to detect edges of a region based on the boundary's parameters set by user and are significantly different from the methods which the background of the region should be segmented. Likewise, most active contour-based approaches are developed from the snake algorithm, which requires the user to identify an initial contour [4]. Thus, these methods are only semi-automatic systems and still suffer from speckle noisein ultrasound images. We need to have a class of objects to determine the accuracy of hemangioma detection and, therefore, catch some initial points by applying preprocessing techniques on ultrasound images [5].

In this paper, we propose an automatic segmentation and boundary delineation system for hemangiomas in ultrasound images of the liver. This solution can be divided into two steps: First, we have an enhancement step which includes image contrast enhancement using modifying the "DoOG'' filter and detection of the region belonging to hemangioma and eliminating undesired regions by "canny" filtering and an adaptive threshold [6, 7] which makes our algorithm more accurate and quicker. Finally, Snake algorithm is applied to segment the exact boundary of the hemangioma for the second step.

A set of ultrasound liver images were used as the dataset for applying our method. The results of images segmented by our method and those by the manual segmentation method were compared. We review other techniques and describe our approach in Section II, discuss our experimental study in Section III, and present concluding remarks in Section IV.

## II. METHODS

The automatic system for hepatic hemangioma boundary segmentation presented in this paper, includes preprocessing modules for image contrast enhancement, a ROI detection, and an edge delineation step [8, 9].

Methods based on deformable contour models such as the Snake algorithm are physically motivated model-based techniques for delineating object boundaries by using closed lines or surfaces that deform under the influence of internal and external forces [10].

For the accurate detection of hemangiomas and to delineate the exact boundaries, 2D Ultrasound images were processed for noise reduction and artifact removal in order to find the suitable ROI for omitting the diaphragm, prior to applying the deformable contour model on the segmentation module. Fig.1 shows the flowchart of this procedure of preprocessing.

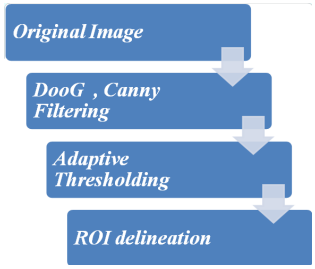


Fig. 1. Pre-processing procedure flowchart

### A. Preprocessing Module

Due to inherent speckles noise and low resolution of the images, the preprocessing module plays a key role in the accurate detection of hemangiomas. It suppresses present noise, enhances feature related information in ultrasound images and makes the follow-up segmentation module more efficient.

The preprocessing module is composed of three algorithms applied at different steps: Gaussian, difference of offset Gaussian (DoOG) and canny detection filter.

The question is to find the independent components in gradient vectors. One of the common ways for illustrating the gradient components is using the difference of offset Gaussian. The DoOG filter, along the X axis, is defined as:

$$DoOG_\sigma(x,y)|_{\theta=0} = G_\sigma(x,y) - G_\sigma(x+d,y) \qquad (1)$$

Where, $G$ is a Gaussian kernel and d is the difference between the centers of two Gaussian filters and is chosen proportional to σ ( as the σ is the variance of the Gaussian function). We can create a family of DoOG functions by rotating the above function in different θ directions:

$$DoOG_\sigma(x,y)|_{\theta=\theta_0} = DoOG_\sigma(x_1,y_1)|_{\theta=0} \qquad (2)$$

Where $y_1 = -x\sin\theta_0 + y\cos\theta_0$ and $x_1 = x\cos\theta_0 + y\sin\theta_0$.

One of the most useful filters to be convolved with digital images is the binomial filter. Through the sequential reiteration, the binomial filter will convert to the Gaussian filter based on the central limit theorem [11]. The Gaussian scale is defined in relation to the number of iterations.

*Canny filter*

The optimized canny edge detection is able to determine most edges in an image using a multi step algorithm. The main characteristics of the canny filter are:

- Optimized detection of edges: the canny filter can detect most actual edges in an image.
- Optimized positioning of edges: the edges, detected by the canny filter, are very close to the actual position of the edges.
- Individual response: the canny filter is able to give an individual response corresponding to each existing edge in the image. Hence, the probability of detecting false edges in the image is reduced.

Using the canny filter, the points of the main edge in the image are better located and have higher color intensity compared to those of the edge points caused by noise. This character can be used to determine the threshold level for color intensity of main edge points and edge points caused by noise. This procedure optimizes the detection of main edge points but the detected real edge line may cause discontinuities. To avoid this problem, canny has used a hysteresis selection method in his suggested approach; if a point has color intensity higher than the threshold level it will be selected instantly. Furthermore, points adjoining a point that has a color intensity between the two threshold levels, $T_h$ and $T_i$, will be selected as main points of the edge. Applying this method reduces the probability that chains of main points become separated [12].

### B. Boundary delineation, Snake (active contour model) algorithm

The snake is an open or closed contour represented parametrically as $C(s) = (x(s), y(s))^T$, where x(s) and y(s) are the coordinates along the contour and $s \in [0,1]$. Each contour form has an energy associated with it, which is placed on an image and moves toward an optimal position and shape, by minimizing its own energy. In our edge delineation module, the snake defines desired image boundaries in an autonomous path by using the internal and external energy forces. The total energy along the contour is

$$E(C) = \int_0^1 \left(E_{\text{int}}(C(s)) + E_{ext}(f, C(s))\right) ds \qquad (3)$$

Where; $E_{int}$ is the internal energy of the area due to bending, and $E_{ext}$ is the background force. The internal force enforces the smoothness, and is derived from the shape of the snake. The external force, on the other hand, attracts the contour to the desired features. The internal energy of the contour depends on the shape of it and can be written as

$$E_{\text{int}} = \left(\alpha(s)|C_s(s)|^2 + \beta(s)|C_{ss}(s)|^2\right)/2 \qquad (4)$$

The first derivative term $\int |C_s(s)|^2 ds$ discourages stretching and makes the model behave like an elastic string or membrane. The second derivative term $\int |C_{ss}(s)|^2 ds$

discourages bending and makes the model behave like a rigid rod or thin plate. These terms are weighted by parameter functions $\alpha(s)$, which controls the tension along the spine (elasticity of the snake), and $\beta(s)$, which controls the rigidity of the spine (stiffness of the snake). In practice, the parameter functions are often chosen to be constants [13]. The external force is a weighted combination of different functions and can be expressed as:

$$E_{ext} = E_{line} + E_{edge} \tag{5}$$

The line-based function $E_{line}$ may be very simple:

$$E_{line} = I(x, y) \tag{6}$$

Where I (x, y) denotes image gray levels at image location (x, y).

The edge-based functional edge attracts the snake to contours with large image gradients, which is to locations with strong edges:

$$E_{ext}(f, C(s)) = -|\nabla f(C)|^2 \tag{7}$$

Where, $\nabla$ f (x, y) calculates the gradient of the enhanced image from the previous module.

## III. EXPERIMENTAL RESULTS AND EVALUATION STATISTICS

The hepatic ultrasound images were from the Sonography Image Processing Lab at "Hazrate Rasoul" Hospital, obtained with the 3-MHz ultrasound probe, at a resolution of 600 × 480 pixels. Thirty five images were used for the verification of the algorithm.

Fig.2 and Fig.3 show the results of the segmentation algorithm in 2D Hepatic Ultrasound images. The image histogram is used for the adaptive thresholding method. Considering the histograms of these images after applying the preprocessing module, the following distribution can be fitted on the histograms as:

$$H(I) = I_{\max} e^{-\alpha(I - I_{\max})} \tag{8}$$

Actually after reaching the peak of histogram $I_{\max}$, the histogram distribution decreases exponentially by the coefficient $\alpha$. For achieving the best threshold we found a suitable point where the magnitude of frequency is 0.04 of the peak in the histogram. To formulate this thresholding method, the following formula is proposed:

$$Threshold = \frac{\log 25}{\alpha} + I_{\max} \tag{9}$$

Using the above can give a good threshold for eliminating non-hemangioma areas. Because hemangiomas are always placed between the Diaphragm and the upper image lobe, determination of a particular area in which the hemangioma can probably exist and applying the suggested procedures, is an effective way to increase the accuracy and pace of the segmentation algorithm.

Fig.2(a) is the original image. After noise removal and image enhancement by the preprocessing module, the output image is shown in Fig.2(b). Fig.3(a) shows the adaptive thresholding on the preprocessed image to find a suitable ROI for the boundary segmentation. The final preprocessing procedure is the outlining of the ROI boundaries and the elimination of lumps in the non-target area of the image. Fig.3(b) shows the resulting ROI contour.

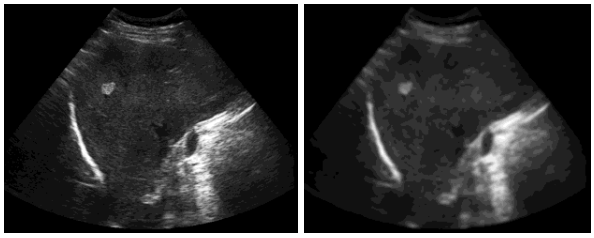

(a) (b)

Fig. 2. (a) Original image, (b) Image after noise removal and enhancement via preprocessing module

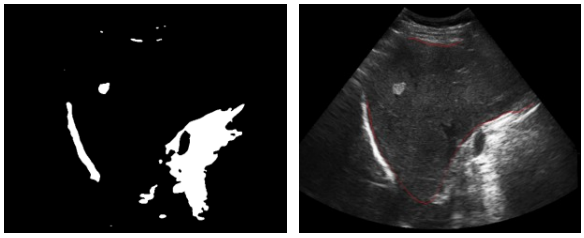

(a) (b)

Fig. 3. (a) Applying adaptive thresholding on the preprocessed image , (b)The resulting ROI contour

Hemangioma segmentation images with manual outlining and computer-aided outlining are presented in Fig.4(a) & (b). It can be seen that the performance of the segmentation module can be significantly improved using the preprocessing module which removes image noise, smoothes images and enhances the image contrast.

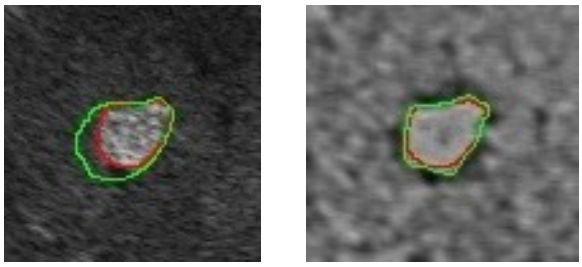

(a) (b)

Fig. 4.Comparison between manually outlined boundary and computer-aided outlining; (a) without preprocessing, (b) after applying preprocessing

The computer-defined boundary on each Ultrasound image was compared with the truth file for evaluation by SM1 and SM2 metrics [14] and Hausdorff distance metrics. SM1 and SM2 metrics are insensitive to area which could be defined as the ratio of the common area between two surfaces to their summation and the Hausdroff distance metric is insensitive to distance. To evaluate the performance of our segmentation module, two area-based metrics [14] and one distance-based metric were used. The evaluation results calculated by the area-based and Hausdroff metrics are shown in TABLE I and

TABLE II. It can be observed that the implementation of the preprocessing module in our algorithm reduces the difference between the boundaries defined by the truth file and the boundaries delineated by the program and the accuracy of the segmentation module has been improved.

TABLE I. Evaluation of automatic segmentation and boundary delineation (using snake) results using the Hausdorff (HD), SM1 and SM2 metrics, with preprocessing

| | SM1 | SM2 | HD | | SM1 | SM2 | HD |
|---|---|---|---|---|---|---|---|
| 1 | 82.1349 | 90.6771 | 2.3540 | 9 | 83.6546 | 90.3148 | 2.8768 |
| 2 | 79.6688 | 90.5689 | 2.9635 | 10 | 83.3493 | 91.4435 | 3.3315 |
| 3 | 83.2507 | 89.7444 | 2.8347 | … | … | … | … |
| 4 | 83.5754 | 89.6225 | 2.5782 | 65 | 83.8564 | 91.3396 | 3.2756 |
| 5 | 80.7071 | 89.7041 | 3.2489 | 66 | 84.7913 | 90.2895 | 2.4501 |
| 6 | 5.3818 | 88.5249 | 3.7442 | 67 | 84.4619 | 91.4789 | 3.0430 |
| 7 | 85.3783 | 89.7660 | 2.7268 | 68 | 84.1557 | 91.1380 | 1.9977 |
| 8 | 82.9247 | 90.1184 | 2.5766 | 69 | 83.0806 | 89.3159 | 2.7535 |
| | | | | **Mean (Std)** | 83.13 (1.87) | 89.88 (0.84) | 2.95 (0.48) |

TABLE II. Evaluation of automatic segmentation and boundary delineation (using snake) results using the Hausdorff (HD), SM1 and SM2 metrics, without preprocessing.

| | SM1 | SM2 | HD | | SM1 | SM2 | HD |
|---|---|---|---|---|---|---|---|
| 1 | 64.6205 | 64.8309 | 5.5003 | 9 | 63.7922 | 73.5710 | 3.6439 |
| 2 | 56.7900 | 69.7867 | 6.8921 | 10 | 69.4420 | 75.5323 | 9.4229 |
| 3 | 72.3656 | 74.3893 | 6.4757 | … | … | … | … |
| 4 | 53.6872 | 72.0711 | 4.1282 | 65 | 62.4309 | 67.7623 | 5.4758 |
| 5 | 36.7479 | 81.5130 | 10.877 | 66 | 47.4341 | 64.3547 | 9.5691 |
| 6 | 47.6836 | 71.0369 | 8.3227 | 67 | 56.5282 | 72.6182 | 7.8055 |
| 7 | 70.5565 | 60.8597 | 10.842 | 68 | 50.5863 | 76.0348 | 8.8749 |
| 8 | 58.8678 | 73.0779 | 5.5068 | 69 | 48.2544 | 70.3571 | 3.8580 |
| | | | | **Mean (Std)** | 58.92 (9.65) | 73.04 (7.63) | 7.26 (2.94) |

The comparison results using SM1, SM2 and Hausdorff metrics with and without preprocessing are presented in Fig.3 and Fig.4.

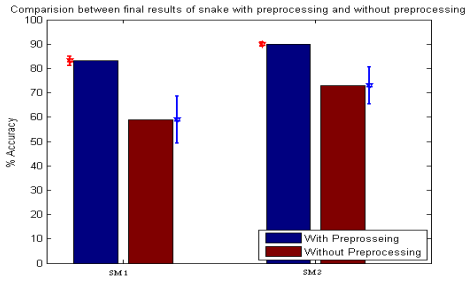


Fig. 3. Comparison of segmentation and boundary delineation (using snake) results using SM1 and SM2 metrics, with and without preprocessing

## I. Conclusion

Semi-automatic or automatic tumor boundary detection methods provide strong, consistent and reproducible results with a certain degree of accuracy. Obviously automatic detection and boundary delineation methods will never replace physicians.

In this study, the preprocessing module which includes DoOG filter for image contrast enhancement was implemented. Finding the ROI using canny edge filter and adaptive thresholding are two steps to help extracting better and more useful features. The resulting images were further segmented by snake algorithm and modified on the 2D hepatic ultrasound images for boundary delineation. It can be observed that the preprocessing module improves accuracy of the segmentation significantly. The evaluation results for this segmentation algorithm show that it is an efficient boundary delineation method among other algorithms.

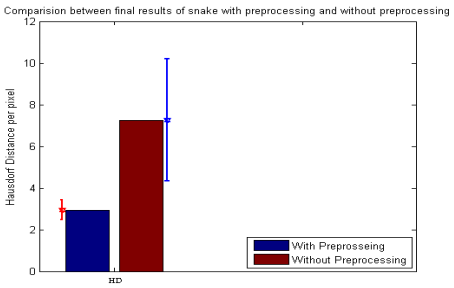


Fig. 4. Comparison of segmentation and boundary delineation (using snake) results using Hausdorff metric, with and without preprocessing.

## References


[1] J.-G. Zheng, Z.-M. Yao, C.-Y. Shu, Y. Zhang, and X. Zhang, "Role of SPECT/CT in diagnosis of hepatic hemangiomas " *World J Gastroenterol,* vol. 11, pp. 5336-5341, 2005.

[2] A. Houston, S. Premkumar, and D. Pitts, "Prostate ultrasound image analysis: localization of cancer lesions to assist biopsy," in *CBMS '95*, Lubbock, TX, 1995, pp. 94-102.

[3] X. Hao, C. Bruce, C. Pislaru, and J. F. Greenleaf, "A Novel Region Growing Method for Segmenting Ultrasound Images," *IEEE Ultraronics Symposium,* vol. 2, pp. 1717 - 1720, 2000.

[4] J. Wang and X. Li, "A System for Segmenting Ultrasound Images," in *proc*: *14th international conference Pattern Recognition*, 1998, pp. 456-461.

[5] Y. Zhanga, R. Sankara, and W. Qianb, "Boundary delineation in transrectal ultrasound image for prostate cancer," *Computers in Biology and Medicine,* vol. 37, pp. 1591-1599, 2007.

[6] K. Krissian, C. Westin, R. Kikinis, and K. Vosburgh, "Oriented speckle reducing anisotropic diffusion," *IEEE Transaction Image Processing,* vol. 32, pp. 1-13, May 2007 2007.

[7] R. M. Haralik, S. Stenberg, and X. Zhuang, "Image analysis using mathematical morphology " *IEEE Transaction Pattern Analysis Machine Intelligence,* vol. 9, pp. 532 - 550, 1987.

[8] W. D. Richard and C. G. Keen, "Automated texture-based segmentation of ulrtasound images of the prostate," *Comput. Med. Imaging Graphics,* pp. 131-140, 1996.

[9] C. B. Burkhardt, "Speckle in ultrasound B-mode scans," *IEEE Transaction Sonics Ultrason.,* vol. 25, pp. 1-6, January 1978 1978.

[10] Y. Zhan and D. Shen, "Automated segmentation of 3D US prostate images using statistical texture-based matching method," in *Lecture Notes in Computer Science*. vol. 2878 Berlin: Springer, 2003, pp. 688-696.

[11] P. S. William, *Adaptive Image Processing*: Boca Raton CRC Press, 2002.

[12] M. Accame and F. G. B. D. Nataleby, "Edge detection by point classification of Canny filtered images " *Signal Processing,* vol. 60, pp. 11-22, 1997.

[13] S. D. Pathak, R. G. Aarnink, J. Rosette, V. Chalana, H. Wijkstra, D. Haynor, F. Debruyne, and Y. Kim, "Quantitative three-dimensional transrectal ultrasound (TRUS) for prostate imaging," *SPIE 3335,* pp. 83-92, 1998.

[14] E. Belogay, C. Cabrelli, U. Molter, and R. Shonkwiller, "Calculating the Hausdorff distance between curves," *Information Processing Letter,* vol. 64 pp. 17-22, 1997.